A Multinuclear Copper(I) Cluster Forms the Dimerization Interface in Copper-Loaded Human Copper Chaperone for Superoxide Dismutase†

Jay P. Stasser, Gnana S. Siluvai, Amanda N. Barry, and Ninian J. Blackburn*

Department of Environmental and Biomolecular Systems, OGI School of Science and Engineering, Oregon Health and Sciences University, Beaverton, OR 97006-8291

Received March 23, 2007; Revised Manuscript Received August 14, 2007

ABSTRACT: Copper binding and X-ray aborption spectroscopy studies are reported on untagged human CCS (hCCS; CCS = copper chaperone for superoxide dismutase) isolated using an intein self-cleaving vector and on single and double Cys to Ala mutants of the hCCS MTCQSC and CSC motifs of domains 1 (D1) and 3 (D3), respectively. The results on the wild-type protein confirmed earlier findings on the CCS−MBP (maltose binding protein) constructs, namely, that Cu(I) coordinates to the CXC motif, forming a cluster at the interface of two D3 polypeptides. In contrast to the single Cys to Ser mutations of the CCS−MBP protein (Stasser, J. P., Eisses, J. F., Barry, A. N., Kaplan, J. H., and Blackburn, N. J. (2005) *Biochemistry 44*, 3143−3152), single Cys to Ala mutations in D3 were sufficient to eliminate cluster formation and significantly reduce CCS activity. Analysis of the intensity of the Cu−Cu cluster interaction in C244A, C246A, and C244/246A variants suggested that the nuclearity of the cluster was greater than 2 and was most consistent with a Cu_4S_6 adamantane-type species. The relationship among cluster formation, oligomerization, and metal loading was evaluated. The results support a model in which Cu(I) binding converts the apo dimer with a D2−D2 interface to a new dimer connected by cluster formation at two D3 CSC motifs. The predominance of dimer over tetramer in the cluster-containing species strongly suggests that the D2 dimer interface remains open and available for sequestering an SOD1 monomer. This work implicates the copper cluster in the reactive form and adds detail to the cluster nuclearity and how copper loading affects the oligomerization states and reactivity of CCS for its partner SOD1.

CCS,[1] the human copper chaperone for superoxide dismutase, is a 27 kDa three-domain protein which functions in the maturation of its target SOD1, the copper/zinc superoxide dismutase (*1*−*4*). Biochemical (*5*, *6*) and crystallographic (*7*−*10*) studies have clarified the structural and functional properties of the individual domains of CCS. Domain 1 (D1) (human, residues 1−77, Figure 1) is an Atx1-like polypeptide which binds a single Cu(I) at the MTX-CXXC motif. Studies in yeast suggest that this domain is only functionally important when cellular copper is depleted (*6*), although in mammalian species it appears to be essential (*11*). Domain 2 (D2) (residues 78−234, Figure 1) is an SOD1-like polypeptide which in the human protein retains its Zn binding site and a vestigial Cu site lacking one of the copper binding histidine residues. This domain is involved in recognition and binding of the SOD1 partner (*5*, *8*). Domain 3 (D3) (residues 235−272) is disordered in the yeast CCS structure (*9*) but becomes well ordered in the yeast heterodimeric complex of CCS with H48F-SOD1 (*8*) and contains a copper binding CXC motif critical to the metal transfer activity of the protein (*5*, *6*). Figure 1 shows the structure of the yeast CCS protein and the sequence of the human protein, with the domains and their corresponding sequences color-coded.

Initial studies suggested that CCS functioned as a classical copper chaperone, activating the EZn form of SOD1 via insertion of the catalytic copper ion. This reaction was first proposed to occur by formation of a CCS−SOD1 heterodimer followed by insertion of the copper-loaded CXC D3 polypeptide into the catalytic center of the EZn-SOD1 (*8*). Recently, however, it has become apparent that CCS function is more complex. The immature apo-SOD1 exists in a monomeric form in which the critical disulfide between C57 and C146 is reduced (*12*) and solvent exposed (*13*). Metalation by CCS is a redox process dependent on the presence of O_2, and it has been shown that, in vivo, CCS converts the reduced EZn^{SH} form to the mature $CuZn^{S-S}$ active enzyme (*14*, *15*) . The mechanism for this process is still unclear, but likely involves redox-mediated thiol−disulfide exchange via the intermediacy of the mixed CCS−

† This work was supported by a program project grant from the National Institutes of Health (P01 GM067166) to N.J.B. We gratefully acknowledge the use of facilities at the Stanford Synchrotron Radiation Laboratory, which is supported by the National Institutes of Health Biomedical Research Technology Program, Division of Research Resources, and by the U.S. Department of Energy, Basic Energy Sciences (BES), and Office of Biological and Environmental Research.

* To whom correspondence should be addressed. N.J.B. Phone: (503) 748-1384. Fax: (503) 748-1464. E-mail: ninian@comcast.net.

[1] Abbreviations: CCS, copper chaperone for superoxide dismutase; CCS−INT, untagged hCCS produced by cleavage of an intein−CCS fusion; D1, domain 1; D2, domain 2; D3, domain 3; DW, Debye−Waller factor; EE-SOD1, superoxide dismutase with both copper and zinc sites empty; EXAFS, extended X-ray absorption fine structure; EZn-SOD1, superoxide dismutase with copper site empty and Zn site full; FT, Fourier transform; hCCS, human CCS; ICP-OES, inductively coupled plasma optical emission spectrometry, MESNA, 2-mercaptoethanesulfonate; SOD, superoxide dismutase; WT, wild type; XAS, X-ray absorption spectroscopy; yCCS, yeast CCS.

10.1021/bi700566h CCC: $37.00
Published on Web 09/29/2007

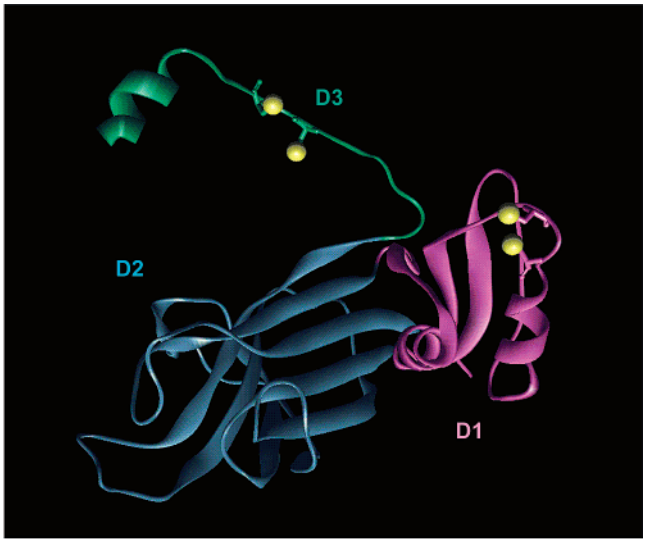

M A S D S G N Q G T L C T L E F A V Q M T **C Q S**
C V D A V R K S L Q G V A G V Q D V E V H L E D
Q M V L V H T T L P S Q E V Q A L L E G T G R Q
A V L K G M G S G Q L Q N L G A A V A I L G G P
G T V Q G V V R F L Q L T P E R C L I E G T I D
G L E P G L H G L H V H Q Y G D L T N N C N S C
G N H F N P D G A S H G G P Q D S D R H R G D L
G N V R A D A D G R A I F R M E D E Q L K V W D
V I G R S L I I D E G E D D L G R G G H P L S K
I T G N S G E R L A C G I I A R S A G L F Q N P
K Q I **C S C** D G L T I W E E R G R P I A G K G R
K E S A

FIGURE 1: Domain structure of CCS. Ribbon diagram of the crystal structure of yCCS (taken from the PDB file 1JK9 for the yCCS−SOD heterodimer where all domains of CCS are ordered). Domain 1 (D1) is shown in magenta, domain 2 (D2) is shown in blue, and domain 3 (D3) is shown in green. The sequence of human CCS corresponding to the three domains is shown below, color-coded D1 magenta, D2 blue, and D3 green. The metal binding cysteine motifs are underlined.

SOD1 disulfide between SOD C57 and yCCS C229, which is observed in the CCS−H48F-SOD1 heterodimer crystal structure.

While providing evidence for a thiol−disulfide isomerase activity of CCS, these studies have provided no information on the role of copper in the process, since the metal is absent in all of the crystal structures. For this reason, we embarked on X-ray absorption spectroscopy (XAS) studies to determine the coordination and nuclearity of copper ligation in human CCS. Previous studies from our laboratory have reported on the XAS of a copper-loaded fusion of CCS and maltose binding protein (CCS−MBP) (*16*, *17*). We determined that copper bound in its Cu(I) form to the two cysteines of the MTCXXC motif in D1 and also formed a cluster involving the CXC motif of D3. Analysis of Cys to Ser mutants in each of these binding sites demonstrated unambiguously that the cluster was formed between two CXC motifs at a D3−D3 dimer interface and hence raised the possibility that Cu(I) cluster chemistry was involved in the redox-mediated disulfide exchange reaction during metal transfer. Specifically, while copper transfer and cluster formation were eliminated by the double Cys to Ser mutants of CXC in D3 (C244/C246S), the analogous C22/C25S mutant of the D1 center retained activity and had the effect of intensifying the 2.72 Å Cu−Cu interaction characteristic of cluster formation. Curiously, single Cys to Ser mutants in either D1 or D3 copper binding sites retained the ability to activate SOD1 and to form Cu(I) clusters.

Protein fusions with large globular proteins such as MBP can potentially affect metal binding properties. In the present paper we report on copper binding and XAS studies of an untagged human CCS construct isolated from an intein self-cleaving vector, CCS−INT. We have also studied single and double Cys to Ala mutants of MTCQSC and CSC of domains 1 and 3, respectively. Our results on the wild-type protein extend our earlier findings on the CCS−MBP constructs. Single Cys to Ala mutations in D3 were now sufficient to eliminate cluster formation and significantly reduce CCS activity. We have also evaluated the relationship among cluster formation, oligomerization, and metal loading. Our results support a model in which Cu(I) binding converts the apo dimer with a D2−D2 interface to a new dimer connected by cluster formation at two D3 CSC motifs. The predominance of dimer over tetramer in the cluster-containing species strongly suggests that the D2 dimer interface remains open and available for sequestering an SOD1 monomer. This work strongly implicates the copper cluster in the reactive form and adds detail to the cluster nuclearity and how copper loading affects the oligomerization states and reactivity of CCS for its partner SOD1.

EXPERIMENTAL PROCEDURES

Cloning and Purification of the Intein−hCCS Fusion and Its Cys to Ala Mutants. Wild-type (WT) hCCS cDNA was PCR-amplified from the maltose binding protein cell line used in our previous studies using primers at the 5′- and 3′-termini (5′-GAATTACCATGGCTTCGGATTCGGGGA-3′ and 5′-AATTTTAAGCTCTTCCGCACGCTGACTCCT-TTCGGC-3′) for the wild-type protein. This expressed the full-length protein minus the last five amino acids (Met1−Ala269). The amplified DNA was cloned into the pTXB3 expression vector (New England Biolabs) using restriction sites *Nco*I and *Sap*I introduced into the 5′ and 3′ PCR primers, respectively. The pTXB3 vector contains an intein/chitin binding protein from the *gyrA* gene of *Mycobacterium xenopi*, which allows the fusion protein to be bound to a chitin bead column and the target protein to be cleaved from the fusion protein by thiol-induced cleavage (*18*, *19*). The truncated form of the protein was PCR-amplified from the same maltose binding protein cell line used in our previous studies using the same primer at the 5′ and a new 3′ primer (5′-GAACTTAAGCTCTTCCGCAGATCTGCTTGGGGT-TCT-3′) to express a protein that terminates right before the CSC motif in D3 (Met1−Ile243).

Mutations to the wild-type hCCS−intein fusion were carried out using a site-directed mutagenesis technique. A Transformer site-directed mutagenesis kit (Clonetech) was used to create single mutants of Cys to Ala (C22A, C25A, C244A, and C246A) in the wild-type expression system described above (*20*). Additionally, two double Ala mutants (C22/25A and C244/246A) were also constructed and expressed. All expression constructs were confirmed by automated DNA sequence analysis.

The intein−hCCS fusion protein was expressed in the *Escherichia coli* strain ER2566 (Novagen) after induction with IPTG with 500 μM $CuSO_4$ and 500 μM $ZnSO_4$ for production of the metalated protein or with no copper added

for the apoprotein (in this study apoprotein refers to a species with no copper and one Zn per monomer). The cells where lysed with a French pressure cell press (SLM-Aminco). The intein−CCS fusion protein was purified from the soluble portion on a chitin bead column. The chitin beads (New England Biolabs) were packed into an XK 16/20 column (Amersham Pharmacia Biotech) and washed with 10 column volumes of column buffer (50 mM sodium phosphate, 500 mM NaCl at pH 7.2). Buffer flow into the column was controlled by gravity. The soluble portion was then diluted three times with column buffer and applied to the column followed by washing with 10 column volumes of column buffer. The column was then washed rapidly with 3 volumes of cleavage buffer (column buffer plus 50 mM 2-mercaptoethanesulfonate (MESNA)) and left to incubate in cleavage buffer overnight at room temperature. Elution was carried out with 4 column volumes of column buffer. The hCCS fractions were analyzed for protein concentration by Bradford assay and metal content by inductively coupled plasma optical emission spectrometry (ICP-OES), and their purity was checked by SDS−PAGE. When necessary, the protein was concentrated with an Amicon centricon ultrafiltration cell.

Cloning and Expression of Human Superoxide Dismutase. EZn-recombinant human SOD was cloned and expressed as described previously (*17*). When necessary, the protein was concentrated with an Amicon centricon ultrafiltration cell. Fully loaded CuZn-SOD was obtained by adding excess $CuSO_4$ to the EZn-SOD followed by dialysis against Cu-free column buffer.

High-Resolution Gel Filtration Chromatography. Freshly prepared hCCs containing 1 mol equiv of Zn and no copper (apo-CCS) was made anaerobic and adjusted to either 10 or 100 μM protein concentration using 50 mM sodium phosphate buffer. Typically, 100 μL of the apoprotein was spun-down through a protein desalting spin column (Pierce) to remove excess MESNA. An aliquot (10 μL) of $Cu(MeCN)_4^+$ dissolved in pure acetonitrile was added such that the final concentration of acetonitrile was 10% and the Cu(I) concentration was between 0 and 3.0 mol equiv. A series of 100 μL protein samples containing 0, 0.5, 1.0, 1.5, 2.0, 2.5, and 3.0 equiv of Cu(I) were allowed to react anaerobically at room temperature for 30 min before being applied to a high-resolution gel filtration column. Volumes of 30 and 5 μL of the protein samples were injected onto the column for proteins of concentrations 10 and 100 μM, respectively. For Co(II) and Zn(II) titrations, aqueous solutions of cobalt(II) perchlorate hexahydrate and zinc(II) sulfate heptahydrate were used.

HPLC gel filtration chromatography was performed with a Varian Prostar solvent delivery module, a Varian Prostar UV/vis detector set at 280 nm, and a Bio-Rad Bio-Sil SEC-250 (7.8 × 300 mm) gel filtration column. Sodium phosphate (50 mM), pH 6.8, containing 500 mM NaCl was used for column equilibration and elution. The molecular weight was determined by comparison to Bio-Rad gel filtration standard no. 151-1901 containing 10 mg/mL bovine thyroglobulin (670 kDa), 10 mg/mL bovine γ-globulin (158 kDa), 10 mg/mL chicken ovalbumin (44 kDa), 5 mg/mL horse myoglobin (17 kDa), and 1 mg/mL vitamin B12 (1.35 kDa). A calibration curve was calculated using the equation

$$R_{av} = \frac{V_e - V_0}{V_t - V_0}$$

where V_e is the elution volume of the sample or standard, V_0 is the void volume, and V_t is the total volume of the column. A plot of R_{av} versus the log of the molecular weight gave a linear calibration curve.

Assay of hCCS Copper Transfer Activity. The assay for the determination of the activity of SOD is the xanthine oxidase assay originally developed by McCord and Fridovich (*21*). Xanthine oxidase catalyzes the conversion of xanthine to urate, which generates high levels of superoxide anion as a byproduct. The amount of superoxide released can be followed by its oxidation of cytochrome *c*, which produces an increase of absorption at 420 nm. The addition of SOD to the reaction mixture removes the superoxide and decreases the oxidation of cytochrome *c*. A unit of SOD is defined as the amount of SOD required to reduce the oxidation of cytochrome *c* by half under standard conditions. The ability of CCS to transfer copper to SOD was measured by incubating apo-SOD with CCS for 15 min at 37 °C in a buffer of 50 mM sodium phosphate containing 10 μM bathrocuproine sulfonate and 10 μM EDTA at pH 7.8. A unit of CCS activity was defined as the amount of CCS required to activate 1 unit of activity of SOD.

Metal Analysis. Copper concentrations were measured by one of two methods throughout these studies, bicinchoninic acid (BCA) assay and ICP-OES. Zinc and cobalt concentrations were routinely measured by ICP-OES. The BCA assay measures the complexation of BCA with copper(I), which forms a purple complex. Protein samples were first mixed with TCA to remove acid-precipitable material such as proteins and other biopolymers and to release all protein-bound copper into the solution. The copper was then reduced by the addition of excess ascorbate and complexed with BCA. The amount of complex formed was determined at 563 or 354 nm and compared to that of standard solutions taken through the identical procedure. ICP-OES was performed on a Perkin-Elmer 2000 Optima DV spectrophotometer. Copper and zinc (or cobalt and zinc) emissions were followed simultaneously and compared to a calibration curve of a multielement standard prepared from stock solutions purchased from Sigma-Aldrich.

XAS Data Collection and Analysis. Cu K edge (8.9 keV) and Zn K edge (9.6 keV) extended X-ray absorption fine structure (EXAFS) and X-ray absorption near edge structure (XANES) data for hCCS and the hCCS mutants were collected at the Stanford Synchrotron Radiation Laboratory operating at 3 GeV with currents between 100 and 50 mA. Data collected on beam line 9-3 used a liquid nitrogen cooled Si[220] monochromator and a Rh-coated mirror upstream of the monochromator with a 13 keV energy cutoff to reject harmonics. A second Rh mirror downstream of the monochromator was used to focus the beam. Samples measured on beam line 7-3 used an unfocused beam with a Si[220] monochromator detuned by 50% to reject harmonics. Data were collected in fluorescence mode using high-count-rate Canberra 30-element Ge array detectors with maximum count rates below 120 kHz. A 6 μ Z-1 metal oxide (Ni, Cu) filter and Soller slit assembly were placed in front of the detector to reduce the elastic scatter peak. Six to nine scans of a

Table 1: Copper and Zinc Binding Ratios to WT hCCS−INT and Its Cysteine to Alanine Single and Double Mutants

	Cu:protein	N^a	Zn:protein	N^a
wild type	1.81 ± 0.13	10	1.02 ± 0.06	8
C22A	0.95 ± 0.02	5	1.04 ± 0.05	5
C25A	1.08 ± 0.15	5	1.05 ± 0.29	5
C244A	0.95 ± 0.15	5	0.90 ± 0.33	5
C246A	0.76 ± 0.11	6	0.95 ± 0.05	5
C22A/25A	0.99 ± 0.06	3	0.89 ± 0.12	3
C244A/246A	0.87 ± 0.12	3	0.95 ± 0.13	3

[a] Number of determinations.

sample containing only sample buffer (20 mM $NaPO_4$, 500 mM NaCl, pH 7.0) were collected at each absorption edge, averaged, and subtracted from the averaged data for the protein samples to remove Z-1 K_β fluorescence and produce a flat preedge baseline. This procedure allowed data of an excellent signal-to-noise ratio to be collected down to 100 μM total copper in the sample. The samples (70 μL) were measured as aqueous glasses (>20% ethylene glycol) at 15 K. Energy calibration was achieved by reference to the first inflection point of a copper foil (8980.3 eV) for Cu K edges and a zinc foil (9660.0 eV) for Zn K edges, placed between the second and third ionization chambers. Data reduction and background subtraction were performed using the program modules of EXAFSPAK (*22*). Data from each detector channel were inspected for glitches, dropouts, and other nonlinear events before inclusion in the final average. Spectral simulation was carried out using the program EXCURVE 9.2 (*23*−*26*) as previously described (*16*, *27*) or the OPT module of EXAFSPAK with the theoretical phase shifts and amplitude functions calculated by FEFF 8.0 (*28*). Both programs gave equivalent results.

RESULTS

Metal Binding. The wild-type hCCS−INT construct purified with an average of 1.81 coppers and 0.92 zinc per monomer (Table 1). These ratios are similar to those of the wild-type CCS−MBP construct, which, when grown in the presence of 500 μM Cu^{2+} and Zn^{2+}, purified with 1.85 coppers and 0.95 zinc per monomer. Mutation of any of the cysteine residues in the MTCQSC or CSC motifs of D1 or D3, respectively, resulted in the binding of one copper per monomer, and unlike the Cys to Ser variants, Cys to Ala mutants (C22A, C25A, C244A, C246A) behaved similarly to double mutants (C22/25A, C244/246A). The mutants showed no change in zinc content, which was always near one Zn per monomer.

Activation of SOD1. The activity of the wild-type hCCS−INT is slightly higher than that of the hCCS−MBP construct (1800 vs 1300 units/mg), possibly due to the loss of the MBP affinity tag. Unlike the MBP constructs in which the single Cys to Ser mutants still showed ∼75% activity, and only the D3 C244/C246S double mutant lost activity, all the hCCS−INT D3 single and double Cys to Ala mutants lost activity. D1 Cys to Ala mutants retained >85% activity, comparable to the results for D1 Cys to Ser mutants in the MBP fusion protein. These data are consistent with the hypothesis that D3 is the critical entity for SOD1 activation and that D1 is not important for activation in vitro.

Copper Cluster Formation Measured by XAS. X-ray absorption edge and EXAFS studies were carried out on the wild-type hCCS−INT, single Cys to Ala mutants C22A, C25A, C244A, and C246A, double Cys to Ala mutants C22/25A and C244/246A, and CCS-I243, a truncation mutant that terminates immediately prior to the CSC D3 copper binding site. For each sample at least two independent data sets were recorded. Metal concentrations for different preparations ranged from 100 to 500 μM. No concentration-dependent differences in spectral features were observed.

Wild-Type hCCS−INT and CCS-I243. Wild-type hCCS−INT gave results (three Cu−S interactions at 2.25 Å, one to two Cu−Cu interactions at 2.72 Å, Table 2, Figure 2) almost identical to those of the wild-type hCCS−MBP, providing good evidence that the copper coordination environment is not significantly affected by the MBP fusion. In contrast, the hCCS-I243 truncation showed no evidence for a second shell in the Fourier transform, confirming our previous observation that cluster formation can only occur with an intact CXC binding site. Acceptable fits to the hCCS-I243 data were obtained with three Cu−S interactions at 2.24 Å. However, only two endogenous Cys residues are available for Cu(I) ligation, and fits with only two Cu−S interactions gave inferior *F* values and distances inconsistent with 2-coordination. 2-coordination was also excluded by the low intensity of the 8983 eV peak on the rising absorption edge (*29*−*31*). Therefore, we explored other fits which assumed coordination by the two endogenous Cys residues and a third ligand, X, which could be either exogenous thiol (left over from the intein cleavage) or solvent oxygen (fits B2 and B3 in Table 2). While neither gives a significant improvement over the unsplit three Cu−S model, the fit with X = S provides a 10% improvement in *F*, suggesting that X is an endogenous thiol. Thus, it would appear that the MTCQSC D1 binding site can bind Cu(I) via the two Cys residues and also recruits a third ligand to complete a 3-coordinate site. Parameters used to fit the data are listed in Table 3.

D3 Mutants C244A, C246A, and C244/246A. Although the D3 mutants purified with one copper per protein, absorption edge measurements (data not shown) indicated that they all contained a mixture of Cu(I) and Cu(II) centers. This could occur if these variants were sensitive to oxidation and could bind copper in D2 either by displacing the Zn ion or at the vestigial Cu site. EXAFS data on these mutants indicated either an all-histidine environment (C244A, three His, one O/N) or a mixed S/N/O shell (C246A, C244/246A). It is possible that the presence of only one coordinating ligand in the CXC motif allows D3 to interact with metal centers in D2, providing a driving force for oxidation to the mixed S/N environment. We found that this anomalous copper binding could be overcome by reducing the samples with dithionite or dithiothreitol as previously described for a CCS−MBP preparation grown in the absence of Zn (*16*). After reduction and exhaustive dialysis the D3 mutants all showed results similar to those of the CCS-I243 truncation, i.e., a 3-coordinate site with two or three Cu−S interactions and no cluster. Parameters used to fit the data are listed in Table 2, fits C and D.

D1 Mutants C22A, C25A, and C22/25A. D1 single and double Cys to Ala mutants did not show the anomalous behavior found for D3 mutants. All mutants were fully reduced and showed two shells of scatterers corresponding to a shell of three Cu−S interactions at 2.26 Å and a shell corresponding to a Cu−Cu interaction at 2.72 Å. In agree-

Table 2: Fits Obtained to the EXAFS of the Cu(I)-Loaded hCCS−INT and Site-Directed Mutants by Curve-Fitting Using the Program EXCURV 9.2

		Cu−S			Cu−O			Cu−Cu			
fit	F^a	CN[b]	R^c (Å)	DW (Å^2)	CN[b]	R^c (Å)	DW (Å^2)	CN[b]	R^c (Å)	DW (Å^2)	$-E_0$
					Wild-Type hCCS						
A1	0.390	3	2.245	0.011				1	2.717	0.012	5.27
A2	0.404	3	2.245	0.010				2	2.720	0.020	5.35
					CCS-I243 Truncation						
B1	0.573	3	2.239	0.015							4.56
B2	0.517	2	2.204	0.007							5.32
		1	2.330	0.003							
B3	0.642	2	2.274	0.012	1	2.037	0.005				10.06
					CCS C244A Dithionite-Reduced						
C1	0.695	3	2.248	0.016							5.63
C2	0.582	2	2.199	0.008							
		1	2.326	0.002							5.35
C3	0.672	2	2.283	0.012	1	2.020	0.005				10.75
					CCS C246A Dithionite-Reduced						
D1	0.592	3	2.258	0.015							5.61
D2	0.485	2	2.212	0.007							5.37
		1	2.338	0.001							
D3	0.621	2	2.293	0.011	1	2.036	0.003				10.57
					CCS C22A						
E1	0.598	3	2.263	0.008				1	2.720	0.003	5.98
E2	0.512	3	2.264	0.007				2.3	2.724	0.012	6.01
					CCS C25A						
F1	0.663	3	2.265	0.009				1	2.724	0.005	6.07
F2	0.553	3	2.266	0.008				2.2	2.726	0.013	6.42
					CCS C244/246A						
G1	0.793	3	2.244	0.014							5.43
G2	0.730	2	2.205	0.006							5.84
		1	2.332	0.002							
G3	0.859	2	2.275	0.012	1	2.044	0.003				10.77
					CCS C22/25A						
H1	0.598	3	2.258	0.008				1	2.724	0.003	5.62
H2	0.425	3	2.262	0.007				2.8	2.730	0.013	6.21

[a] F is a least-squares fitting parameter defined as $F^2 = (1/N)\sum_{i=1}^{N} k^6(\text{data} - \text{model})^2$. [b] Coordination numbers are generally considered accurate to ±25%. [c] In any one fit, the statistical error in bond lengths is ±0.005 Å. However, when errors due to imperfect background subtraction, phase-shift calculations, and noise in the data are compounded, the actual error is probably closer to ±0.02 Å.

ment with previous data on the CCS−MBP C22/25S variant, the intensity of the second-shell feature had increased relative to that of wild-type hCCS−INT. The second-shell Cu−Cu feature was best fit by scattering from at least two Cu−Cu interactions, suggesting a cluster nuclearity greater than 2. Parameters used to fit the data are listed in Table 2, fits E, F, and G. The persistence of an intense feature due to Cu−Cu interaction in mutants which lack the D1 copper binding site provides compelling evidence for D3−D3 dimerization via a domain-spanning Cu(I) cluster.

A comparison of the EXAFS of FTs of the D1 and D3 mutants is shown in Figures 3 and 4 for the single and double Cys to Ala mutants respectively.

Cluster Formation as a Function of Copper Loading. Apo-CCS was titrated with increasing amounts of Cu(I) to produce samples containing 0, 0.5, 1, 1.5, and 2 mol equiv of Cu(I) per monomer. The copper-loaded samples were analyzed by EXAFS to determine the relationship among copper coordination, cluster formation, and copper loading. Each sample was fitted to a two-shell model comprising three Cu−S interactions and a variable occupancy of Cu−Cu with the DW ($2\sigma^2$) set to 0.013 Å^2. The Cu:protein = 0.5 sample showed a Fourier transform with three Cu−S interactions at 2.24 Å that was essentially identical to that of the D1 Ala mutants or the CCS-I243 truncation described above. Refinement of the Cu−Cu interaction gave values between 0 and 0.2. At Cu:P = 1, the second-shell feature became observable in the FT, corresponding to a 2.72 Å Cu−Cu interaction at 0.3 shell occupancy. At Cu:P = 1.5 and 2, the Cu−Cu interaction increased markedly in a nonlinear sigmoidal fashion characteristic of cooperative behavior. Figure 5 shows Fourier transforms as a function of copper loading, with a plot of the second-shell intensity versus copper loading as an inset. The sigmoidal nature of the curve suggests that Cu(I) loads first into the mononuclear (D1) center but subsequent loading into the D3 sites drives the cluster formation to completion. This process may involve protein conformational changes and/or recruitment of D1-bound Cu(I) ions into D3 cluster formation.

Activity versus Copper Loading. We tested the SOD1 activation activity of hCCS as a function of copper loading. To ensure that the measured activity was based on the ability of the different copper-loaded forms to transfer copper to SOD, and not on the overall copper concentration, the amount of hCCS added was enough to maintain a constant Cu:SOD1 ratio of 2:1. Therefore, with Cu:hCCS = 0.5, 4 times the amount of hCCS was incubated with SOD1, while, with the Cu:hCCS = 2 sample, the ratio of CCS:SOD1 was 1:1. Under these conditions, the 0.5 ratio sample gave an activity of 450 units/mg, greatly reduced from that of the

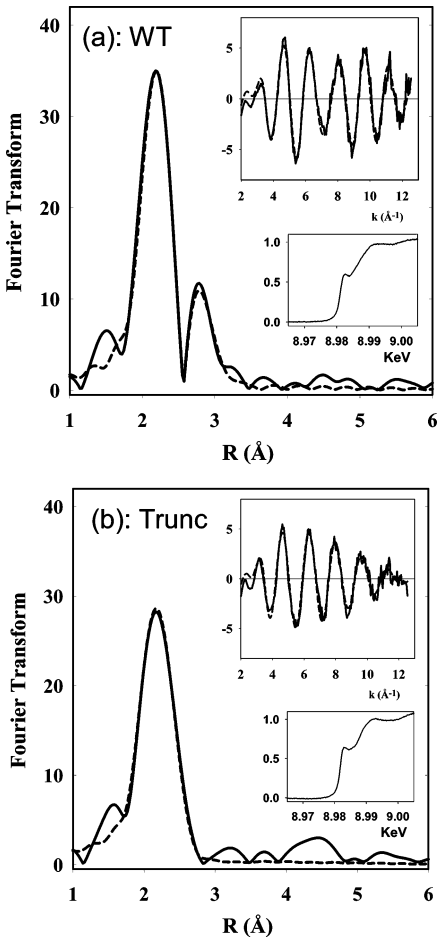

FIGURE 2: Comparison of Fourier transforms, EXAFS, and absorption edges for (a) wild-type hCCS−INT and (b) the I243 truncation mutant. Solid lines are experimental data, and dashed lines are simulated data. Parameters used in the simulations are tabulated in Table 2.

wild-type protein, while the activities of the 1, 1.5, and 2 ratio samples were 860, 1700, and 1900 units/mg. The results normalized to unity for the Cu:P = 2 sample are also plotted in the inset to Figure 5 and show a remarkable correlation with the presence of the Cu−Cu cluster.

Oligomerization. It is clear from the XAS data of the Cys to Ala mutants that cluster formation only occurs when Cu(I) binds to the CXC residues in D3, which implies that the cluster provides a template for dimerization at the D3−D3 interface. However, apo-hCCS has been shown to associate into dimers using the SOD-like D2−D2 interface (*10*), which raises the question of how further dimerization via D3 affects the oligomeric state of the protein. Therefore, we investigated the oligomerization behavior of hCCS as a function of copper loading, using high-resolution gel filtration. Figure 6 shows HPLC traces for WT hCCS and the C22/25A (D1) and C244/246A (D3) double mutants. All samples were 10 μM on the basis of the monomeric MW and were loaded anaerobically with increasing amounts of Cu(I) from 0 to 3.0 mol equiv. As previously reported, WT apoprotein exists almost exclusively as a dimer with a peak position of 60 kDa relative to molecular weight markers (MW_{calcd}(hCCS monomer) = 28 400).

Addition of Cu(I) to hCCS leads to variable oligomerization equilibria depending on the state of copper loading and on the presence of mutations in domains 1 and 3. For the WT protein, addition of Cu(I) induces the appearance of a tetrameric fraction (apparent MW = 133 000) which maximizes between 2 and 2.5 equiv of Cu(I). A low concentration of higher order oligomer is also detectable. At Cu(I) concentrations above 2.0 equiv, the tetramers and oligomers convert back to dimer. The tetrameric species persists in the D1 mutant, but is not present in the D3 mutant series, regardless of the Cu(I) concentration, allowing it to be assigned to Cu(I) binding to the D3 CXC binding site and hence presumably to polypeptide cross-linking via the Cu cluster. Similar oligomerization patterns were observed at higher concentration (100 μM) (Figure S1, Supporting Information), with the difference that higher concentrations of tetramer and oligomer relative to dimer were observed. However, at the highest Cu(I) concentrations, these higher order complexes likewise were reconverted cleanly and reversibly to dimers.

While it seems probable that the tetramer is induced by Cu cluster formation, the role of the cluster in the dimer structure is less clear. Further, it is not necessary that the dimers observed throughout the titration all be derived from the *same* dimerization interface. For example, while the apo dimer is known to use the D2−D2 interface, the metal-bound (holo dimers) could equally well associate via the D3 cluster (or both interfaces) with no change in molecular size (Figure 7). To gain further insight into the nature of the dimers, we isolated the dimer and tetramer peaks, reran them on the HPLC sizing column, and compared their Cu to protein ratios. When rechromatographed, dimers and tetramers gave single peaks and did not reequilibrate during the time scale of the experiment (3−4 h). The results are shown in Table 3. The copper content (per monomer) of the tetrameric fraction (at the end point of the titration) is 2.7 for the WT and 1.6 for the D1 mutant, consistent with a higher order cluster as suggested from XAS. Whereas the dimer fractions generally contain less copper during the early and midpoints of the titration (suggesting the expected coexistence of apo and holo dimers), they also approach values for the WT between 2.5 and 3 Cu atoms per monomer as at the highest Cu levels where all tetramer has converted to dimer. The D1 mutant copper ratios approach values of 2−1 less mol equiv of copper per monomer than in the WT—due to the absence of the D1 binding site. These data strongly suggest that the dimer species also contains the higher order Cu cluster.

Co(II) has been shown to bind to human and tomato CCS where it was postulated to form a 4-coordinate mononuclear tetrahedral complex (*32*). The suggested mode of binding implicated two Cys residues from D1 and D3. Therefore, Co(II) would not be expected to form a cluster at the D3−D3 interface, such that only dimers but not tetramers or oligomers would be expected. To test this hypothesis, we titrated Co(II) and Zn(II) into hCCS and separated the products by HPLC to assess the oligomeric states induced by these metal ions. The dimeric composition of the apoprotein was unaffected by either metal at ratios between 0.5 and 3.0. Identical results were obtained at 10 and 100 μM (Figures S2 and S3, Supporting Information). For each metal, the dimer peaks observed at nominal metal:protein ratios of 1.0, 2.0, and 3.0 were separated and analyzed for Co(II) and Zn(II) content (Table 3). The Co(II) ratios were found to be substoichiometric with values of ~0.3 per

Table 3: Metal Binding Ratios for Dimer and Tetramer Fractions Formed during Titration of Apo-hCCS with Cu(I) and Co(II)[a]

		wild type		C22/25A		C244/246A	
metal	metal:P	dimer	tetramer	dimer	tetramer	dimer	tetramer
Cu(I)	1.0			0.65 ± 0.01	1.19 ± 0.06	0.90 ± 0.06	
Cu(I)	1.5	1.34 ± 0.17	1.59 ± 0.03	1.14 ± 0.01	1.43 ± 0.06		
Cu(I)	2.0	1.80 ± 0.04	2.00 ± 0.11	1.22 ± 0.07	1.62 ± 0.13	1.42 ± 0.16	
Cu(I)	2.5	2.21 ± 0.23	2.68 ± 0.13				
Cu(I)	3.0	2.76		1.85			
Co(II)	1.0	0.25		0.19			
Co(II)	2.0	0.32		0.34			
Co(II)	3.0	0.29		0.41			

[a] Standard deviations refer to duplicate determinations. In cases where no standard deviation is given, only a single determination was made. At Cu:P = 3 the tetramer is almost completely converted back to dimer such that no value of the tetramer copper content can be made.

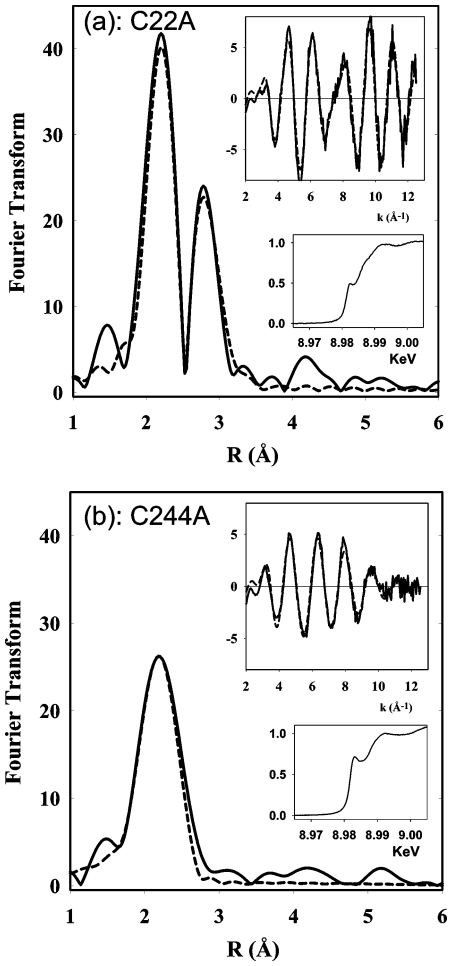

FIGURE 3: Comparison of Fourier transforms, EXAFS, and absorption edges for (a) C22A hCCS−INT and (b) C244A hCCS−INT. Solid lines are experimental data, and dashed lines are simulated data. Parameters used in the simulations are tabulated in Table 2.

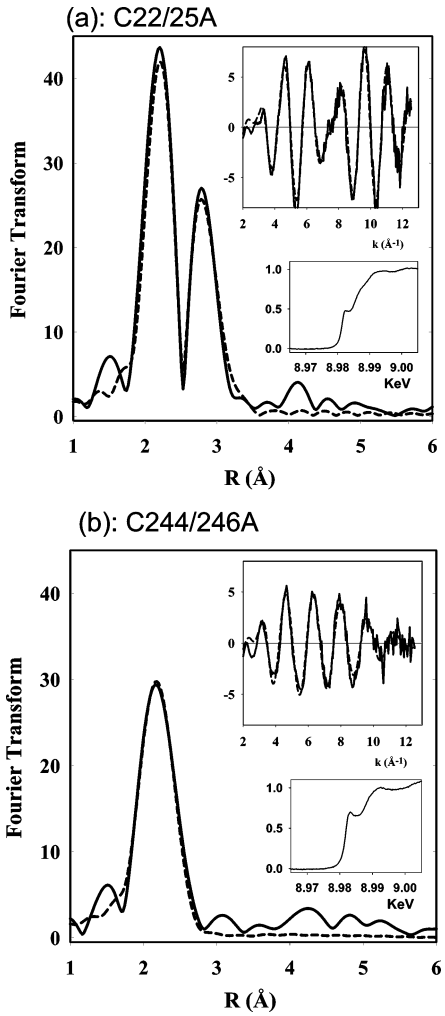

FIGURE 4: Comparison of Fourier transforms, EXAFS and absorption edges for (a) C22/25A hCCS−INT and (b) C244/246A hCCS−INT. Solid lines are experimental data, and dashed lines are simulated data. Parameters used in the simulations are tabulated in Table 2.

monomer for both the WT and the C22/25A mutant. Zn(II) levels did not increase above the one Zn per monomer characteristic of the apoprotein. These data suggest that neither Co(II) nor Zn(II) is able to reproduce the tetramer/oligomer formation and that the latter is a unique property of the native Cu(I) ion.

DISCUSSION

We have shown that the untagged WT CCS protein binds copper in a manner similar to that of the previously characterized MBP fusion protein. CCS grown in the presence of 500 μM Cu and Zn was isolated with two Cu atoms and one Zn atom per monomer, and subsequent XAS and EXAFS analysis showed that the copper was bound in the Cu(I) oxidation state. As before, the EXAFS spectrum of the WT protein was composed of a first shell of three Cu−S interactions at the expected distance of 2.25 Å and a second shell of one to two Cu−Cu interactions at 2.72 Å. We also studied a series of site-directed mutants in which one or both of the Cys residues at each of the copper binding sites were mutated to Ala. These mutants had altered activity

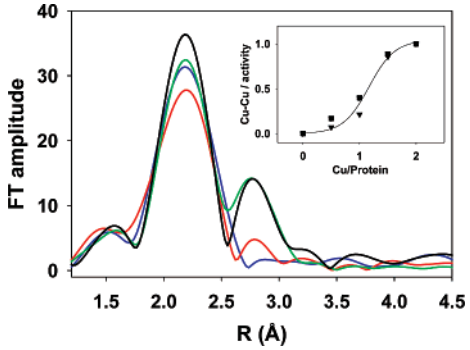

FIGURE 5: Fourier transforms of wild-type hCCS−INT loaded with increasing amounts of Cu(I). Copper:protein ratios were as follows: blue trace, 0.5; red trace, 1; green trace, 1.5; black trace, 2. The inset shows the relationship between the Cu:protein ratio and (▼) the intensity of the Cu−Cu shell in the transform determined by simulation and normalized to the value at Cu:P = 2 and (■) the copper transfer activity normalized to the maximum activity at Cu:P = 2, corrected for the residual activity of the C244/246A double mutant.

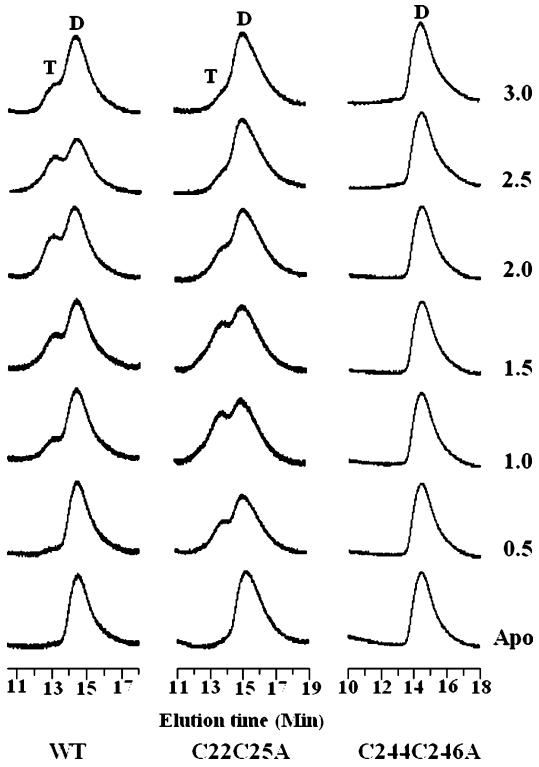

FIGURE 6: High-resolution gel filtration chromatograms of 10 μM hCCS−INT and its C22/25A (D1) and C244/246A (D3) mutants obtained upon addition of 3.0 equiv of $[Cu(CH_3CN)_4]PF_6$ in steps of 0.5 equiv. "D" and "T" represent the dimer and tetramer, respectively.

and/or copper binding characteristics. Mutations in D3 (C244A, C246A, and C244/246A) and the D3 truncation (CCS-I243) lost both the metal transfer activity and the second-shell Cu−Cu interaction, whereas mutations in D1 (C22A, C25A, C22/25A) retained >85% of their activity and exhibited a more intense second-shell feature. Studies using partially loaded forms of CCS showed that the apoprotein and the fully loaded protein were both dimeric, but most likely had different dimer interfaces. We propose that the apoprotein dimerizes at the SOD-like D2 dimer interface, while the metalated protein dimerizes via the D3 copper cluster, perhaps leaving an open D2 interface for

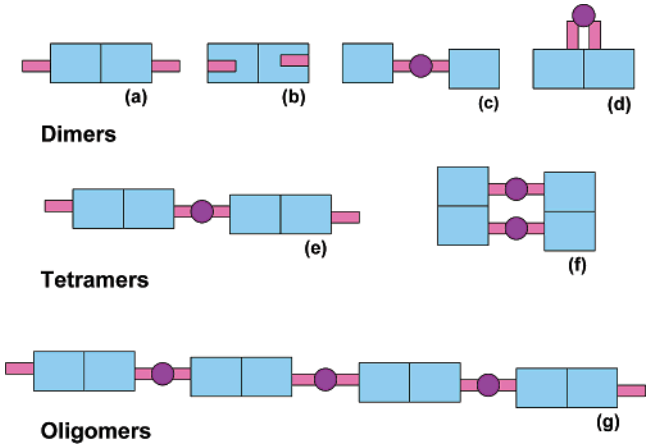

FIGURE 7: Possible forms of the oligomeric hCCS molecular isoforms: (a) apo dimer with no cluster and a D2−D2 interface, (b) dimer with an intramolecular D1−D3 cluster and a D2−D2 interface, (c) dimer with an intermolecular cluster and a D3−D3 interface, (d) dimer species cross-linked at both interfaces, (e) tetramer linking dimer species in (a) via one intermolecular D3−D3 cluster, (f) tetramer linking dimer species in (a) via two D3−D3 clusters, (g) a possible oligomeric structure.

association with further CCS molecules, or with the SOD1 partner. Further, both cluster formation and copper transfer activity are nonlinear functions of copper loading and appeared to be correlated, suggesting a relationship between the extent of cluster formation and SOD1 activation.

Nature of the hCCS Copper Cluster. Given the above evidence that SOD activation is correlated with cluster formation, the chemistry of the activation process is likely to depend critically on the cluster composition and geometry. The EXAFS of the copper centers in CCS is a simple two-shell system, but significant insight into the cluster geometry can be gleaned from comparison of the outer shell intensities and fitting parameters for WT CCS and its variant forms. For example, if only the WT spectrum is considered, it is difficult to draw firm conclusions as to cluster composition, since there are two potential copper binding sites, and both could conceivably contribute to the cluster. However, when the D1 and D3 mutants are compared, it is clear that the cluster resides entirely within D3, since mutation of the D1 Cys residues, or truncation of the protein prior to the CXC D3 binding site, eliminates the cluster completely. Thus, in analyzing the structure of the cluster, we need to examine the simulation parameters of the C22/25A double mutant, which rigorously excludes any contribution from D1 Cys residues. When the EXAFS of this variant is critically analyzed, the second shell can (as usual) be fit by a variety of combinations of shell occupancy and DW factor, ranging from one Cu−Cu interaction at 2.72 Å with DW ($2\sigma^2$) = 0.003 Å^2 (F = 0.598), to four Cu−Cu interaction at 2.73 Å with DW ($2\sigma^2$) = 0.018 Å^2 (F = 0.422). If the shell occupancy and DW for the second shell are refined together, the "best fit" is 2.8 Cu−Cu interactions at 2.73 Å with DW ($2\sigma^2$) = 0.013 Å^2 (F = 0.425). If the one Cu−Cu shell occupancy is further examined, it becomes apparent that the Cu−Cu DW factor is half that of the Cu−S shell ($2\sigma^2$ = 0.006) and is much smaller than usually found in structurally characterized Cu−S clusters (*31*).

Table 4 lists Cu−Cu nuclearities, distances, and DW factors ($2\sigma^2$) for a number of Cu−S clusters described in

Table 4: Shell Occupancy, Cu−Cu Distances, and Debye−Waller Factors ($2\sigma^2$) for Copper−Thiolate Clusters in Models and Proteins

complex	N_{Cu-Cu}	R_{Cu-Cu} (Å)	DW (Å^2)	ref
hCCS C22/25A	2.8	2.724	0.013	this work
Cu_4S_6 model	3	2.741	0.0150	*31*
Cu_5S_7 model	0.8	2.696	0.0100	*31*
Cu_5S_6 model	2.4	2.725	0.0134	*31*
Ace1	2	2.704	0.0172	*33*
	1	2.902	0.0176	
Mac1	2	2.705	0.0176	*33*
	1	2.891	0.0178	
Ctr1	2	2.715	0.0132	*34*
	1	2.898	0.0142	
Cox17	1.2	2.705	0.0104	*44*
Cox11	1	2.706	0.0080	*49*
Cu_A mixed-valence	1	2.43	0.0020	*35*
Cu_A reduced	1	2.51	0.0070	*35*
Cu_A mixed-valence model	1	2.93	0.0130	*35*
average[a]			0.0124	

[a] The average Cu−Cu DW factor was computed for the reduced Cu(I)−thiolate systems only. In cases exhibiting two Cu−Cu interactions, only the 2.7 Å distance was included.

the literature. These systems fall into three categories: Cu_xS_y multinuclear clusters, Ace1, Mac1, and the C-terminal domain of yeast Ctr1 with Cu−Cu DW factors in the range 0.010−0.018 Å^2 (*31*, *33*, *34*), Cox11 and Cox17 where the nuclearity is unknown, but with DW factors between 0.008 and 0.014 Å^2, and the mixed-valence or fully reduced, bis-thiolate-bridged dicopper clusters found in the Cu_A center of cytochrome *c* oxidase (*35*, *36*) with significantly lower values of $2\sigma^2$. For the latter system, the DW factor of mixed-valence Cu_A is similar to that of the $N = 1$ Cu−Cu interaction model of the CCS D3 cluster. However, the low DW factors for the Cu_A center are unique as they reflect the presence of an extremely short Cu−Cu distance in both oxidation states (*35*−*38*) and a metal−metal bond in the mixed-valence form (*39*−*41*). It thus seems reasonable to predict that the DW factor for the cuprous thiolate cluster in CCS should approach the average of the DW factors for the systems in Table 4, but excluding the mixed-valence centers of cytochrome oxidase. This average gives an expected value of 0.0124 Å^2 for the CCS cluster. On the basis of these arguments, it appears that the D3 cluster nuclearity must be greater than 2. Of great significance, when the shell occupancy and DW factor for the C22/25A variant of CCS are refined, the minimum is obtained at three Cu−Cu interactions with a DW of 0.013 Å^2, in good agreement with the other clusters of Table 4.

The most common multinuclear Cu(I)−thiolate clusters are based on the Cu_4S_6 adamantane-type structure which is composed of three Cu_3S_3 hexagonal rings fused together (*42*). As shown in Figure 8A, the Cu(I) centers are 3-coordinate and have three neighboring Cu(I) centers, with each Cu(I) ion bridged to its neighbor by a thiolate S. The Cu−Cu separation is ∼2.7 Å. This cluster thus exhibits all of the structural features identified from analysis of the C22/25A CCS XAS data. Clearly there are many other ways that multinuclear Cu(I) clusters could be assembled, but of those reported in the Cambridge database, few have nuclearities less than 3. As discussed by Pickering and co-workers (*31*), other more complex clusters such as Cu_5S_7 or Cu_5S_6 also contain longer Cu−Cu distances at ∼2.9−3.0 Å, which have been identified in the EXAFS of the transcriptional activators Ace1 and Mac1 (*33*), but these longer distances appear to be absent in the CCS cluster, as addition of extra Cu−Cu scattering around 3 Å degrades the fit.

Although the Cu_4S_6 cluster clearly fits well to the EXAFS data, a major difficulty is that it requires two copper and three sulfur atoms per D3 monomer. Copper loading of dimer and tetramer fractions is indeed consistent with two coppers per D3 binding site, but D3 contains only two Cys residues per monomer, and a third Cys residue is more problematic. D2 contains two Cys residues—C141 and C227—which form a homologous disulfide to the critical disulfide in hSOD1 (*10*, *43*), and two other Cys residues, C113 and C144. The heterodimer structure of yCCS complexed with the H48F-ySOD1 partner (*8*) shows that a mixed disulfide forms between CCS D3 residue C229 and C57 (C244 and C57, hCCS numbering). This may suggest that the homologous C141 of hCCS may participate in the D3 copper cluster and further that the homologous C57 of reduced (immature) hSOD1 may itself participate in a complex cluster within the active heterodimeric or heterotetrameric complex as a precursor to SOD1 disulfide formation (*12*, *14*).

In contrast to the single Cys to Ala mutations described in the present paper, we previously reported that C244 or C246 could be substituted by serine without disrupting the integrity of the cluster (*17*). These mutants retained activity provided the CCS was present in excess. This observation can be rationalized in the context of a multinuclear cluster, since thiol residues at opposing corners could be substituted for hydroxyl without cluster decomposition. Similar behavior has been observed in Cu(I)-loaded Cox17 (*44*), as is well documented in Fe/S cluster chemistry (*45*).

The HPLC data allow us to assess the likelihood of possible oligomeric structures as shown in Figure 7. Copper-dependent dimerization has been noted before in both yeast and human CCS. yCCS is monomeric in the apo form but forms a mixture of monomers and dimers on binding up to two coppers per monomer (*6*). hCCS on the other hand has been shown to be dimeric in both the apo form (*10*, *43*) and in a copper-loaded form containing 1.2 coppers per monomer produced by copper addition followed by exhaustive dialysis against chelators (*43*). These previous studies did not document the relationship between copper loading and cluster formation, and our present work sheds light on this issue. Four different forms of the dimeric protein can be postulated, an apo dimer with no cluster and a D2−D2 interface (Figure 7a), an intramolecular D1−D3 cluster with a D2−D2 interface (Figure 7b), an intermolecular D3−D3 cluster with a D3−D3 interface, (Figure 7c), and a species cross-linked at both interfaces (Figure 7d). Our results show that at high Cu:P, the dimer fraction has close to three Cu atoms per monomer in the WT and two Cu atoms per monomer in the C22A/C25A mutant. This dimer species must therefore contain the copper cluster, and the data are entirely consistent with the Cu_4S_x formulation derived from the EXAFS analysis, suggesting that (c) or (d) is most likely. The tetrameric proteins which form solely as a consequence of the presence of the cluster must have two independent association interfaces as depicted by (e) and (f) in Figure 7. The structure in (e) contains only one copper cluster and thus would have a lower Cu:monomer ratio. It is likely that this would be the initial tetramer species to form at lower Cu:P ratios. As Cu:P rises (Table 3), the structure in (e) could

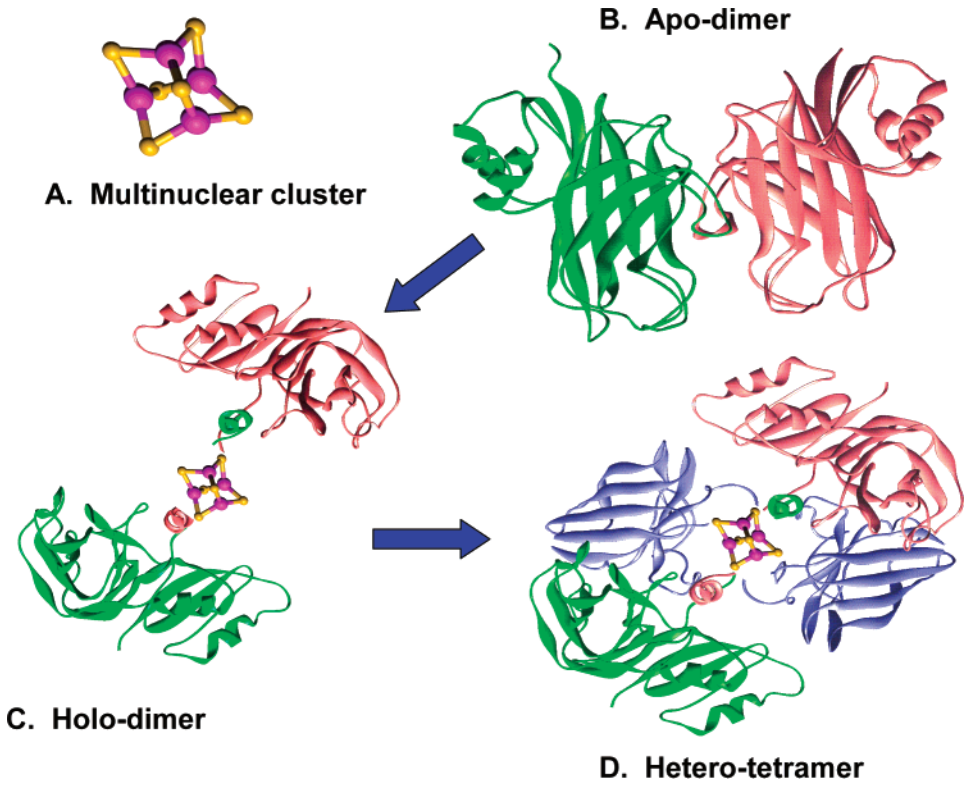

FIGURE 8: Structure-based model for the copper-induced CCS target recognition. (A) Possible structure for a tetranuclear Cu(I) cluster with metrical parameters consistent with the EXAFS analysis. (B) Apo-hCCS is a dimer, with an interaction at the SOD-like D2−D2 interface. (C) When loaded with Cu(I), rearranges into a new dimeric species, via cluster formation at the D3 interface. (D) This leaves the D2 dimer interface open for complex formation with the incoming SOD1 target protein. (The structure of the apo dimer in (A) was taken from PDB file 1QUP. The structure of the copper-induced dimer in (B) was adapted from the yCCS−H48F-SOD1 heterodimer (1JK9) with the SOD1 chains deleted. The structure of the heterotetramer complex in (C) was adapted from the yCCS−SOD1 structure 1JK9).

convert to the structure in (f) or to the oligomeric structure in (g).

The mechanism by which tetramers (and oligomers) convert to dimers at high Cu:P ratios is presently obscure. However, the dimers that are formed still retain the copper cluster, suggesting that the primary mechanism is the disruption of the D2−D2 interface. Thus, for example, if the tetramer in (f) dissociated into a dimer by disruption of the D2−D2 interaction, the structure in (c) would be generated. Further, it is unlikely that the dimer in (d) could form without significant strain within the molecule to bring both interfaces into alignment for association. We therefore propose that the structure in (c) is the most likely option for the dimer formed at higher copper to protein ratios.

For these results to be relevant to the situation inside the cell, it is important to compare the in vitro concentrations used in this study to estimations of hCCS abundance in vivo. Rae et al. (*46*) estimated that, in yeast, there are 10^4 yCCS monomers in a cell volume of 10^{-14} L. A simple calculation gives an estimated 10^{-19} mol of CCS per cell, leading to a yCCS concentration of 10 μM. In the present study, hCCS concentrations used for XAS were in the range 100−500 μM, well above the expected abundance of cellular CCS. Data described here, and in a previous report (*16*), have shown that the outer shell features of the Cu(I) cluster are fully developed at the lowest CCS concentrations measured and do not change as the Cu concentration increases. In parallel, we have shown by HPLC analysis that Cu(I) cluster formation is responsible for tetramer formation since only dimers are formed in the D1 Cys to Ala double mutants and in the Co(II) reconstituted systems. The fact that tetramers are clearly seen in HPLC profiles at 10 μM hCCS therefore implies that the Cu(I) cluster persists at a concentration which is physiologically relevant. Further, if the copper-loaded dimers are indeed D3−D3-associated species as the analysis suggests, then the cluster must be the dominant Cu(I) species present at physiological concentrations.

Our results can be related to a mechanism for CCS function as follows. At Cu:protein ≥ 2, hCCS contains a copper cluster which is formed by dimerization of two D3 polypeptides. While it is possible that this protein has two sites of dimerization at the D2 and D3 interfaces, a more plausible scenario is that it represents a dimeric form *different* from that of the apoprotein. In this scenario, copper binding and cluster formation convert the apo dimer (associated at the SOD-like D2 interface) into a new dimer species formed through the D3−D3 interface, with the D2 dimer interface open and able to form tetramers via further dimerization at the D2 interface or to bind an SOD molecule. This process would provide an ideal way for hCCS to capture its target, as the open D2 interface which interacts with SOD would only become available after the protein began to load with copper (Figure 8B−D). Conformational changes associated with copper loading have been well documented on the basis of differences in proteolysis (*6*, *43*). The molecular changes associated with copper binding appear to be highly metal specific, as Co(II) and Zn(II), which are known to form stable tetrathiolate complexes, are unable to generate the oligomerization functionality.

Recent studies on regulation of hCCS by copper add support to these conclusions. Intracellular CCS levels are inversely proportional to the cellular copper concentrations and are regulated by a mechanism which is independent of the activity of the CTR1 importer (*11*, *47*, *48*). Of particular interest, Gitlin and co-workers have demonstrated that increasing copper levels lead to molecular changes which allow the CCS to be targeted for proteosomal degradation, and these changes are associated with the CXC cluster-forming motif in D3, since mutation of this motif abrogated the sensitivity to Cu (*11*). Moreover, the double mutant hCCS Y134E/G135E, a variant known to have a disrupted D2−D2 dimer interface (*5*), exhibits more rapid turnover than the WT protein, suggesting that the D2−D2 dimer interface must be open for recognition by the proteosomal machinery. These results imply that increasing copper concentration leads to disruption of the D2−D2 dimer interface by a mechanism which directly involves the CXC D3 motif and provide strong support for the conclusions of the present study. Taken together, they suggest a critical role for the Cu(I) cluster in breaking the D2−D2 interaction, allowing access for both SOD1 association and proteosomal targeting.

Further work is under way to clarify these processes and to gain additional insight into the structure and function of the CCS multinuclear Cu(I) cluster.

ACKNOWLEDGMENT

We thank Dr. Michiko Nakano and Mary Mayfield Gambill for help with the construction and expression of mutant proteins.

SUPPORTING INFORMATION AVAILABLE

High-resolution gel-filtration chromatographs for the metal-dependent oligomerization of WT and mutant forms of hCCS at various protein concentrations: Figure S1, Cu(I)-dependent oligomerization at 100 μM hCCS; Figure S2, Co(II)- and Zn(II)-dependent oligomerization at 10 μM hCCS; Figure S3, Co(II)- and Zn(II)-dependent oligomerization at 100 μM hCCS. This material is available free of charge via the Internet at http://pubs.acs.org.

REFERENCES

1. Culotta, V. C., Klomp, L. W. J., Strain, J., Casareno, R. L. B., Krems, B., and Gitlin, J. (1997) The copper chaperone for superoxide dismutase, *J. Biol. Chem. 272*, 23469−23472.
2. Culotta, V. C., Yang, M., and O'Halloran, T. V. (2006) Activation of superoxide dismutases: Putting the metal to the pedal, *Biochim. Biophys. Acta 1763*, 747−758.
3. Huffman, D. L., and O'Halloran, T. V. (2001) Function, structure, and mechanism of intracellular copper trafficking proteins, *Annu. Rev. Biochem. 70*, 677−701.
4. Rosenzweig, A. C. (2001) Copper delivery by metallochaperone proteins, *Acc. Chem. Res. 34*, 119−128.
5. Schmidt, P. J., Kunst, C., and Culotta, V. C. (2000) Copper activation of superoxide dismutase 1 (SOD1) *in vivo*. Role for protein-protein interactions with the copper chaperone for SOD1, *J. Biol. Chem. 275*, 33771−33776.
6. Schmidt, P. J., Rae, T. D., Pufahl, R. A., Hamma, T., Strain, J., O'Halloran, T. V., and Culotta, V. C. (1999) Multiple protein domains contribute to the action of the copper chaperone for superoxide dismutase, *J. Biol. Chem. 274*, 23719−23725.
7. Hall, L. T., Sanchez, R. L., Holloway, S. P., Zhu, H., Stine, J. E., Lyons, T. J., Demeler, B., Schirf, V., Hansen, J. C., Nersissian, A. M., Valentine, J. S., and Hart, P. J. (2000) X-ray crystallographic and ultracentrifugation analyses of truncated and full-length copper chaperones for SOD (LYS7). A dimer-dimer model of LYS7-SOD association and copper delivery, *Biochemistry 39*, 3611−3623.
8. Lamb, A. L., Torres, A. S., O'Halloran, T. V., and Rosenzweig, A. C. (2001) Heterodimeric structure of superoxide dismutase in complex with its metallochaperone, *Nat. Struct. Biol. 8*, 751−755.
9. Lamb, A. L., Wernimont, A. K., Pufahl, R. A., Culotta, V. C., O'Halloran, T. V., and Rosenzweig, A. C. (1999) Crystal structure of the copper chaperone for superoxide dismutase, *Nat. Struct. Biol. 6*, 724−729.
10. Lamb, A. L., Wernimont, A. K., Pufahl, R. A., O'Halloran, T. V., and Rosenzweig, A. C. (2000) Crystal structure of the second domain of the human copper chaperone for superoxide dismutase, *Biochemistry 39*, 1589−1595.
11. Caruano-Yzermans, A. L., Bartnikas, T. B., and Gitlin, J. D. (2006) Mechanisms of the copper-dependent turnover of the copper chaperone for superoxide dismutase, *J. Biol. Chem. 281*, 13581−13587.
12. Arnesano, F., Banci, L., Bertini, I., Martinelli, M., Furukawa, Y., and O'Halloran, T. V. (2004) The unusually stable quaternary structure of human Cu,Zn-superoxide dismutase 1 is controlled by both metal occupancy and disulfide status, *J. Biol. Chem. 279*, 47998−48003.
13. Banci, L., Bertini, I., Cantini, F., D'Amelio, N., and Gaggelli, E. (2006) Human SOD1 before harboring the catalytic metal: solution structure of copper-depleted, disulfide-reduced form, *J. Biol. Chem. 281*, 2333−2337.
14. Furukawa, Y., Torres, A. S., and O'Halloran, T. V. (2004) Oxygen-induced maturation of SOD1: a key role for disulfide formation by the copper chaperone CCS, *EMBO J. 23*, 2872−2881.
15. Brown, N. M., Torres, A. S., Doan, P. E., and O'Halloran, T. V. (2004) Oxygen and the copper chaperone CCS regulate posttranslational activation of Cu,Zn superoxide dismutase, *Proc. Natl. Acad. Sci. U.S.A. 101*, 5518−5523.
16. Eisses, J. F., Stasser, J. P., Ralle, M., Kaplan, J., and Blackburn, N. J. (2000) Domains I and III of the human copper chaperone for superoxide dismutase interact via a cysteine-bridged dicopper cluster, *Biochemistry 39*, 7337−7342.
17. Stasser, J. P., Eisses, J. F., Barry, A. N., Kaplan, J. H., and Blackburn, N. J. (2005) Cysteine-to-serine mutants of the human copper chaperone for superoxide dismutase reveal a copper cluster at a domain III dimer interface, *Biochemistry 44*, 3143−3152.
18. Chong, S., Mersha, F. B., Comb, D. G., Scott, M. E., Landry, D., Vence, L. M., Perler, F. B., Benner, J., Kucera, R. B., Hirvonen, C. A., Pelletier, J. J., Paulus, H., and Xu, M. Q. (1997) Single-column purification of free recombinant proteins using a self-cleavable affinity tag derived from a protein splicing element, *Gene 192*, 271−281.
19. Telenti, A., Southworth, M., Alcaide, F., Daugelat, S., Jacobs, W. R., and Perler, F. B. Jr. (1997) The Mycobacterium xenopi GyrA protein splicing element: characterization of a minimal intein, *J. Bacteriol. 179*, 6378−6382.
20. Carter, P. (1987) Improved oligonucleotide-directed mutagenesis using m13 vectors, *Methods Enzymol. 154*, 382−403.
21. McCord, J. M., and Fridovich, I. (1969) Superoxide dismutase. An enzyme function for erythrocuprein (hemocuprein), *J. Biol. Chem. 244*, 6049−6055.
22. George, G. N. (1990) EXAFSPAK, Stanford Synchrotron Radiation Laboratory, Menlo Park, CA.
23. Binsted, N., Gurman, S. J., and Campbell, J. W. (1998) EXCURVE 9.2, Daresbury Laboratory, Warrington, England.
24. Gurman, S. J., Binsted, N., and Ross, I. (1984) A rapid, exact, curved-wave theory for EXAFS calculations, *J. Phys. C 17*, 143−151.
25. Gurman, S. J., Binsted, N., and Ross, I. (1986) A rapid, exact, curved-wave theory for EXAFS calculations. II. The multiple-scattering contributions, *J. Phys. C 19*, 1845−1861.
26. Binsted, N., and Hasnain, S. S. (1996) State of the art analysis of whole X-ray absorption spectra, *J. Synchrotron Radiat. 3*, 185−196.
27. Blackburn, N. J., Rhames, F. C., Ralle, M., and Jaron, S. (2000) Major changes in copper coordination accompany reduction of peptidylglycine monooxygenase, *J. Biol. Inorg. Chem. 5*, 341−353.
28. Zabinsky, S. I., Rehr, J. J., Ankudinov, A. L., Albers, R. C., and Eller, M. J. (1995) Multiple-scattering calculations of x-ray-absorption spectra, *Phys. Rev. B 52*, 2995−3009.

29. Ralle, M., Cooper, M. J., Lutsenko, S., and Blackburn, N. J. (1998) The Menkes disease protein binds copper via novel 2-coordinate Cu(I)-cysteinates in the N-terminal domain, *J. Am. Chem. Soc. 120*, 13525−13526.
30. Ralle, M., Lutsenko, S., and Blackburn, N. J. (2004) Copper transfer to the N-terminal domain of the Wilson disease protein (ATP7B). X-ray absorption spectroscopy of reconstituted and chaperone-loaded metal binding domains and their interaction with exogenous ligands, *J. Inorg. Biochem. 98*, 765−779.
31. Pickering, I. J., George, G. N., Dameron, C. T., Kurz, B., Winge, D. R., and Dance, I. G. (1993) X-ray absorption spectroscopy of cuprous-thiolate clusters in proteins and model systems, *J. Am. Chem. Soc. 115*, 9498−9505.
32. Zhu, H., Shipp, E., Sanchez, R., Liba, A., Stine, J. E., Hart, P. J., Gralla, E. B., Nersissian, A. M., and Valentine, J. S. (2000) Co(2+) binding to human and tomato copper chaperone for superoxide dismutase: Implications for the metal ion transfer mechanism, *Biochemistry 39*, 5413−5421.
33. Brown, K. R., Keller, G. L., Pickering, I. J., Harris, H. H., George, G. N., and Winge, D. R. (2002) Structures of the cuprous-thiolate clusters of the Mac1 and Ace1 transcriptional activators, *Biochemistry 41*, 6469−6476.
34. Xiao, Z., Loughlin, F., George, G. N., Howlett, G. J., and Wedd, A. G. (2004) C-terminal domain of the membrane copper transporter Ctr1 from Saccharomyces cerevisiae binds four Cu(I) ions as a cuprous-thiolate polynuclear cluster: sub-femtomolar Cu(I) affinity of three proteins involved in copper trafficking, *J. Am. Chem. Soc. 126*, 3081−3090.
35. Blackburn, N. J., de Vries, S., Barr, M. E., Houser, R. P., Tolman, W. B., Sanders, D., and Fee, J. A. (1997) X-ray Absorption studies on the mixed-valence and fully reduced forms of the soluble Cu_A domains of *Thermus thermophilus* and *Bacillus subtilis* cytochrome *c* oxidase: Structural evidence for minimal electron transfer reorganizational energy, *J. Am. Chem. Soc. 119*, 6135−6143.
36. Williams, P. A., Blackburn, N. J., Sanders, D., Bellamy, H., Stura, E. A., Fee, J. A., and McRee, D. E. (1999) The Cu_A domain of *Thermus thermophilus* ba_3- type cytochrome *c* oxidase at 1.6 Å resolution, *Nat. Struct. Biol. 6*, 509−516.
37. Iwata, S., Ostermeier, C., Ludwig, B., and Michel, H. (1995) Structure at 2.8 A resolution of cytochrome *c* oxidase from *Paracoccus denitrificans*, *Nature 376*, 660−669.
38. Tsukihara, T., Aoyama, H., Yamashita, E., Tomizaki, T., Yamaguchi, H., Shinzawa-Itoh, K., Nakashima, R., Yaono, R., and Yoshikawa, S. (1995) Structures of metal sites of oxidized bovine heart cytochrome c oxidase at 2.8 A resolution, *Science 269*, 1069−1074.
39. Gamelin, D. R., Williams, K. R., Lacroix, L. B., Houser, R. P., Tolman, W. B., Mulder, M. C., de Vries, S., Hedman, B., Hodgson, K. O., and Solomon, E. I. (1997) The influence of copper-sulfur covalency and copper-copper bonding on valence delocalization and electron transfer in the Cu_A site of cytochrome *c* oxidase, *J. Am. Chem. Soc. 119*, 613−614.
40. Gamelin, D. R., Randall, D. W., Hay, M. T., Houser, R. P., Mulder, T. C., Canters, G. W., de Vries, S., Tolman, W. B., Lu, Y., and Solomon, E. I. (1998) Spectroscopy of mixed-valence Cu_A centers: ligand field control of ground state properties related to electron transfer, *J. Am. Chem. Soc. 120*, 5246−5263.
41. Glaser, T., Hedman, B., Hodgson, K. O., and Solomon, E. I. (2000) Ligand K-edge X-ray absorption spectroscopy: a direct probe of ligand-metal covalency, *Acc. Chem. Res. 33*, 859−868.
42. Dance, I. G., and Calabrese, J. C. (1976) The crystal and molecular structure of the hexa-(μ_2-benzenethiolato)tetracuprate(I) dianion, *Inorg. Chim. Acta 19*, L41−L42.
43. Rae, T. D., Torres, A. S., Pufahl, R. A., and O'Halloran, T. V. (2001) Mechanism of Cu, Zn-superoxide dismutase activation by the human metallochaperone hCCS, *J. Biol. Chem. 276*, 5166−5176.
44. Heaton, D. N., George, G. N., Garrison, G., and Winge, D. R. (2001) The mitochondrial copper metallochaperone Cox17 exists as an oligomeric polycopper complex, *Biochemistry 40*, 743−751.
45. Flint, D. H., and Allen, R. M. (1996) Iron−Sulfur Proteins with Nonredox Functions, *Chem. Rev. 96*, 2315−2334.
46. Rae, P. J., Schmidt, P. J., Pufahl, R. A., Culotta, V. C., and O'Halloran, T. V. (1999) Undetectable intracellular free copper: the requirement of a copper chaperone for superoxide dismutase, *Science 284*, 805−808.
47. Bertinato, J., and L'Abbe, M. R. (2003) Copper modulates the degradation of copper chaperone for Cu,Zn superoxide dismutase by the 26 S proteosome, *J. Biol. Chem. 278*, 35071−35078.
48. Bartnikas, T. B., and Gitlin, J. D. (2003) Mechanisms of biosynthesis of mammalian copper/zinc superoxide dismutase, *J. Biol. Chem. 278*, 33602−33608.
49. Carr, H. S., George, G. N., and Winge, D. R. (2002) Yeast Cox11, a protein essential for cytochrome *c* oxidase assembly, is a Cu(I)-binding protein, *J. Biol. Chem. 277*, 31237−31242.

BI700566H